CORA Cork Open Research Archive
Cartlann Taighde Oscailte Chorcaí

Title	Laterally coupled distributed feedback lasers emitting at 2μm with quantum dash active region and high-duty-cycle etched semiconductor gratings
Authors	Papatryfonos, Konstantinos;Saladukha, Dzianis;Merghem, Kamel;Joshi, Siddharth;Lelarge, Francois;Bouchoule, Sophie;Kazazis, Dimitrios;Guilet, Stephane;Le Gratiet, Luc;Ochalski, Tomasz J.;Huyet, Guillaume;Martinez, Anthony;Ramdane, Abderrahim
Publication date	2017-02-01
Original Citation	Papatryfonos, K., Saladukha, D., Merghem, K., Joshi, S., Lelarge, F., Bouchoule, S., Kazazis, D., Guilet, S., Gratiet, L. L., Ochalski, T. J., Huyet, G., Martinez, A. and Ramdane, A. (2017) 'Laterally coupled distributed feedback lasers emitting at 2μm with quantum dash active region and high-duty-cycle etched semiconductor gratings', Journal of Applied Physics, 121, 053101 (8pp). doi:10.1063/1.4975036
Type of publication	Article (peer-reviewed)
Link to publisher's version	10.1063/1.4975036
Rights	© 2017, the Authors. Reproduced with the permission of AIP Publishing from Journal of Applied Physics 121, 053101; doi: 10.1063/1.4975036
Download date	2024-10-16 15:24:20
Item downloaded from	https://hdl.handle.net/10468/3954

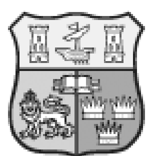
UCC
University College Cork, Ireland
Coláiste na hOllscoile Corcaigh

.

Laterally coupled distributed feedback lasers emitting at 2 μm with quantum dash active region and high-duty-cycle etched semiconductor gratings

Konstantinos Papatryfonos, Dzianis Saladukha, Kamel Merghem, Siddharth Joshi, Francois Lelarge, Sophie Bouchoule, Dimitrios Kazazis, Stephane Guilet, Luc Le Gratiet, Tomasz J. Ochalski, Guillaume Huyet, Anthony Martinez, and Abderrahim Ramdane

Citation: J. Appl. Phys. **121**, 053101 (2017); doi: 10.1063/1.4975036

View online: http://dx.doi.org/10.1063/1.4975036

View Table of Contents: http://aip.scitation.org/toc/jap/121/5

Published by the American Institute of Physics

Articles you may be interested in

Iron doped InGaAs: Competitive THz emitters and detectors fabricated from the same photoconductor
J. Appl. Phys. **121**, 053102053102 (2017); 10.1063/1.4975039

High harmonic generation in ZnO with a high-power mid-IR OPA
J. Appl. Phys. **110**, 061101061101 (2017); 10.1063/1.4975362

Photonic crystal properties of self-assembled Archimedean tilings
J. Appl. Phys. **121**, 023101023101 (2017); 10.1063/1.4973472

Long-range Tamm surface plasmons supported by graphene-dielectric metamaterials
J. Appl. Phys. **121**, 033101033101 (2017); 10.1063/1.4973900

AIP | Journal of Applied Physics

INTRODUCING INVITED PERSPECTIVES

Ultrafast magnetism and THz spintronics

Authors: Jakob Walowski and Markus Münzenberg

RIGHTSLINK

JOURNAL OF APPLIED PHYSICS **121**, 053101 (2017)

Laterally coupled distributed feedback lasers emitting at 2 μm with quantum dash active region and high-duty-cycle etched semiconductor gratings

Konstantinos Papatryfonos,[1,a)] Dzianis Saladukha,[2,3] Kamel Merghem,[1] Siddharth Joshi,[4,b)] Francois Lelarge,[4,b)] Sophie Bouchoule,[1] Dimitrios Kazazis,[1,c)] Stephane Guilet,[1] Luc Le Gratiet,[1] Tomasz J. Ochalski,[2,3] Guillaume Huyet,[2,3,5] Anthony Martinez,[1] and Abderrahim Ramdane[1]

[1]*CNRS Laboratory for Photonics and Nanostructures, Route de Nozay, 91460 Marcoussis, France*
[2]*Tyndall National Institute, Lee Maltings, Dyke Parade, Cork, Ireland*
[3]*Centre for Advanced Photonics and Process Analysis, Cork Institute of Technology, Cork, Ireland*
[4]*III-V Lab, a Joint Lab of "Alcatel Lucent Bell Labs," "Thales Research and Technology," and "CEA Leti," Route de Nozay, 91460 Marcoussis, France*
[5]*National Research University of Information Technologies, Mechanics and Optics, St. Petersburg, Russia*

(Received 12 November 2016; accepted 17 January 2017; published online 1 February 2017)

Single-mode diode lasers on an InP(001) substrate have been developed using $InAs/In_{0.53}Ga_{0.47}As$ quantum dash (Qdash) active regions and etched lateral Bragg gratings. The lasers have been designed to operate at wavelengths near 2 μm and exhibit a threshold current of 65 mA for a 600 μm long cavity, and a room temperature continuous wave output power per facet >5 mW. Using our novel growth approach based on the low ternary $In_{0.53}Ga_{0.47}As$ barriers, we also demonstrate ridge-waveguide lasers emitting up to 2.1 μm and underline the possibilities for further pushing the emission wavelength out towards longer wavelengths with this material system. By introducing experimentally the concept of high-duty-cycle lateral Bragg gratings, a side mode suppression ratio of >37 dB has been achieved, owing to an appreciably increased grating coupling coefficient of $\kappa \sim 40\,cm^{-1}$. These laterally coupled distributed feedback (LC-DFB) lasers combine the advantage of high and well-controlled coupling coefficients achieved in conventional DFB lasers, with the regrowth-free fabrication process of lateral gratings, and exhibit substantially lower optical losses compared to the conventional metal-based LC-DFB lasers. *Published by AIP Publishing.*
[http://dx.doi.org/10.1063/1.4975036]

I. INTRODUCTION

Monolithic semiconductor lasers are attractive components for monitoring the environment, utilizing infrared absorption spectroscopy for gas sensing. Devices based on low-dimensional structures such as self-assembled quantum dots (QDs) and quantum dashes (Qdashes) are promising candidates for this application, owing mainly to their size and composition fluctuations resulting after their epitaxial growth. As a result, such nanostructures exhibit a wider gain spectrum than mainstream quantum wells (QWs), thus providing possibilities for wide-range tunability and multi-species gas analysis using a single laser.[1,2] In recent years, considerable attention has been given to InAs Qdashes,[3] which are elongated nanostructures grown on the InP(001) substrate, with the dimensions of their cross-section being similar to that of a shallow quantum dot ($\sim$2–3 nm $\times$ 15–20 nm), and their length in the $[1\bar{1}0]$ direction being of the order of 200–300 nm. We have recently performed a detailed investigation of the fundamental electronic properties of $InAs(P)/In_{0.78}Ga_{0.22}As_{0.47}P_{0.53}$ Qdashes using cross-sectional scanning tunneling microscopy and spectroscopy, where we have shown that they exhibit a 1-D quantum-wire-like electronic density of states.[4] However, since their length is significantly shorter than that of nanowires, they possess certain advantages with respect to laser applications, mainly arising from their reduced active volumes. In particular, advanced laser characteristics, such as high modal gain, relatively low threshold current, low internal losses, and high output power, have been recently demonstrated at 1.55 μm for applications in telecommunications[5–7] as well as at longer emission wavelengths.[8–10] Furthermore, it is worth mentioning that Qdashes may also find applications beyond lasers, as single photon sources emitting at 1.55 μm, further exploiting their quantum properties.[11]

The fact that the emission wavelength of Qdashes can be tuned based on their size,[12] can particularly benefit gas sensing applications, which require well-controlled emission wavelengths to match the specific absorption lines of different gases. In fact, within our work, we find that by also changing the barrier material and carefully optimizing the growth conditions of the new structure, a further shift of the emission wavelength may be achieved and high-performance lasers emitting above 2 μm are obtained while maintaining a binary InAs Qdash composition. The wavelength range around 2 μm is of particular interest as well as some important gases, such as CO_2 and NH_3, exhibit strong absorption lines. While alternative approaches using different material systems are available for 2-μm lasing, most notably by

[a)]Author to whom correspondence should be addressed. Electronic mail: constantinos.papatryfonos@lpn.cnrs.fr
[b)]Current address: Almae Technologies, site Data4, Route de Nozay, Marcoussis, France.
[c)]Current address: Laboratory for Micro- and Nanotechnology, Paul Scherrer Institute, 5232 Villigen-PSI, Switzerland.

RIGHTSLINK

taking the advantage of the QW technology in Sb-based materials[13,14] or by utilizing type-II QWs on the InP(001) substrate,[15,16] during this work, we will focus our attention on InAs/InP Qdashes. Due to the fact that they can be grown self-assembled on InP(001) and related lattice-matched material, Qdashes can directly benefit from the growth and processing technologies that have been mastered through the development of telecommunications lasers, while, as compared to the latter approach of type-II QWs, they can maintain appreciably lower threshold current densities. On the other hand, it is also possible to achieve a long wavelength emission with very satisfying performances by using highly strained type-I QWs on InP,[17] but investigating low-dimensional nanostructures deserves attention as it may ultimately provide opportunities for wide-range tunability.

Given an optimized material structure, subsequent processing of single-frequency distributed feedback (DFB) or distributed Bragg reflector (DBR) lasers with high single longitudinal mode purity is a prerequisite for high-resolution absorption spectroscopy. In order to achieve this, various different approaches have been reported to date, including successful demonstrations in wavelength performance, but also certain trade-offs. The conventional approach that is mainly used in telecom applications employs a growth interruption, during which a Bragg grating is patterned and etched, with the required upper epitaxial layers subsequently overgrown on top of it. Even though this approach is highly reliable and well known, these multiple growth techniques require additional complex processing steps, thus increasing the manufacturing cost and introducing yield and reliability problems. For semiconductor lasers to become more attractive in the gas sensing industry, as well as in other applications where cost consideration is an important factor, a substantial process simplification should be a high priority. For this reason, in recent years, the re-consideration of regrowth-free DFB lasers, where the grating is formed after or during the definition of the waveguide, has drawn considerable attention. In this approach, the index modulation interacts with the lateral optical fields (evanescent fields) to provide the optical feedback, which may cause these structures to suffer from low coupling efficiencies, unless special treatment is provided. In their early demonstrations, such lasers utilizing lateral feedback, have been referred to as corrugated ridge waveguide (CRW) or as laterally coupled distributed feedback (LC-DFB) lasers and included variations in which the grating was etched on the ridge,[18] exclusively in the ridge sidewalls (CRW),[19] exclusively beside the ridge (LC-DFB),[20] or over both regions.[21] More recently, LC-DFB lasers using metallic gratings have also been given particular attention and subsequently used in the industrial applications, as a result of their higher coupling coefficient—induced by the additional periodic loss of the periodic metallic structures, making these lasers mainly gain (loss)-coupled DFB lasers.[22–25] In additional recent work, improvements in low-loss, high-power operation have been achieved by etched lateral grating fabrication,[13] or by use of a two-step ridge etch process for minimal lateral current spreading.[26] On the other hand, higher side mode discrimination in relatively short cavities has been achieved by operation with a narrower ridge waveguide of 1.7 μm width,[27] introducing first-order[28,29] or optimized third-order[30–34] Bragg gratings on the ridge waveguide sidewalls, or by use of focused ion beam lithography (FIB) in LC-DFB[35] and LC-DBR[36,37] configurations. Notably, chirped CRW gratings for the better control over the coupling coefficient have been also investigated.[38,39] However, the simultaneous achievement of a high coupling coefficient and low grating-induced losses in a regrowth-free design remained a challenge for both CRWs and LC-DFBs. Resolving this challenge is of great importance for future laser applications, which require a combination of a low manufacturing cost with a high side mode suppression ratio (SMSR) and a low threshold current for low power consumption. In this letter, we demonstrate Qdash based LC-DFB lasers emitting around 2.0 μm. High grating coupling coefficients ($\kappa \sim 40\,\mathrm{cm}^{-1}$) that result in the high side mode discrimination of >37 dB for relatively short gratings (375 μm), together with negligible grating-induced losses, are provided by high-duty-cycle etched Bragg gratings, which are implemented experimentally in such lateral configuration for the first time. Furthermore, this process is applied on a novel heterostructure design that is promising for future sensing applications.

II. SAMPLE PREPARATION

The studied structure was grown by a gas source molecular beam epitaxy (GSMBE) on an n-doped InP(001) substrate. The nominally undoped active region consisted of six InAs Qdash layers separated by 40 nm thick ternary alloy $In_{0.53}Ga_{0.47}As$ barriers and was sandwiched between two thicker (80 nm) $In_{0.53}Ga_{0.47}As$ waveguide layers. On top of the upper waveguide layer, the following epi-layers were successively grown: a 100 nm thick InP spacer layer, a 35 nm $In_{0.78}Ga_{0.22}As_{0.47}P_{0.53}$ layer dedicated for the Bragg grating definition, a p-doped 1.5 μm InP cladding layer, and a p+-doped 0.3 μm InGaAs ohmic contact layer. By inserting Qdash nanostructures directly in such a low barrier (absorption etch at $\lambda = 1.65\,\mu$m) in replacement of the conventional InGaAsP ($\lambda = 1.17\,\mu$m) barrier, in a dash-in-a-barrier (DBar)[5] structure, we achieved a further shift of the emission wavelength. This shift resulted from the lower confining potential, which leads to less confined electronic wave functions within the quantum dash and thus to lower energies. For our studied epi-wafer with the largest grown Qdashes, lasing has been observed at ~2.08 μm, which is a record lasing wavelength for Qdash based approaches. Notably, this is already achieved without changing the Qdash composition, using binary InAs Qdashes. In addition, such a low barrier results in a reduction of the laser threshold current; however, for applications requiring high output power, an intermediate barrier is instead preferable as it is expected to provide higher slope efficiencies.[40] In fact, for high current injection in the continuous wave (CW) regime, thermal roll-over limits the maximum output power per facet to ~5.5 mW for the best lasers, in our low-barrier structures. Nevertheless, for the targeted sensing applications, such values are more than sufficient. While the long-wavelength results underline the potential of this approach for reaching

RIGHTSLINK

the milestones of 2.3 and 2.55 μm in the near future, possibly using InAsSb Qdashes[41] embedded in a laser structure identical to the one described above,[42] or in the dashes-in-a-step-well approach,[43] in the remaining of this paper, we will analyze the results of a slightly different sample that includes somewhat smaller Qdashes, emitting around 2 μm. This wavelength is particularly interesting for the detection of NH_3. We identified the optimum wavelength for detection of this gas at 1.982 μm, based on the relevant NH_3, CO_2, and H_2O absorption peaks in this spectral region. Therefore, our LC-DFB lasers described hereafter were particularly designed for targeting this application. The photoluminescence (PL) peak of the sample is at 1.98 μm.

100-μm-wide broad area (BA) lasers were initially processed in order to test the material quality. A threshold current density of $\sim$1.6 kA/cm^2 has been measured for devices with the cavity length of $\sim$600 μm. By assessing BA lasers with cavity lengths varying from 400 μm to 1.5 mm, a high modal gain of the order of 45 cm^{-1} and internal losses of 18 cm^{-1} were extracted. Subsequently, 2.0-μm-wide ridge-waveguide lasers were fabricated in order to validate the gain peak position and to assure single-transverse-mode operation.

III. LC-DFB LASER DESIGN

Then, prior to single-mode laser fabrication, numerical investigations were carried out in order to identify the optimum design. In the various studied approaches, we find that a new method for achieving LC-DFBs with a high SMSR, based on lateral high-duty-cycle etched semiconductor Bragg gratings, is particularly prominent. As it is shown below, such gratings may provide sufficient feedback while not being a source of additional losses to the laser, in contrast to their metallic counterparts, or the CRWs. Moreover, due to the obtained high grating coupling coefficients, the desired SMSR values may already be achieved for the short grating sections, thus providing nice possibilities for LC-DFBs with short cavities and paving the way for low-loss LC-DBR lasers. The duty cycle (w/Λ) of a Bragg grating is defined as the semiconductor portion (w) of a grating period (Λ), shown schematically in Fig. 1(a). According to the coupled mode theory, the coupling coefficient of a rectangular-shaped grating may be written as[44]

$$\kappa = \frac{(n_1^2 - n_2^2)}{n_{eff}\lambda} \frac{\sin\left(\frac{m\pi w}{\Lambda}\right)}{m} \Gamma_{grating}, \quad (1)$$

where n_1 and n_2 are the refractive indices of the semiconductor and the dielectric material that compose the grating (Fig. 1(a)), n_{eff} is the effective index of the guided mode, λ is the wavelength in free space, Λ is the grating period, m is the relevant grating diffraction order, and $\Gamma_{grating}$ is the field overlap integral with the grating region. It is important that such a simulation is performed in a computationally efficient way, in order to enable investigating a variety of structures of interest. For this reason, we first used the eigenmode expansion method to compute the modal effective index and the electric field distribution in order to obtain numerical n_{eff} and $\Gamma_{grating}$ values and subsequently substituted them in Eq. (1). An example fundamental quasi-TE mode profile of a

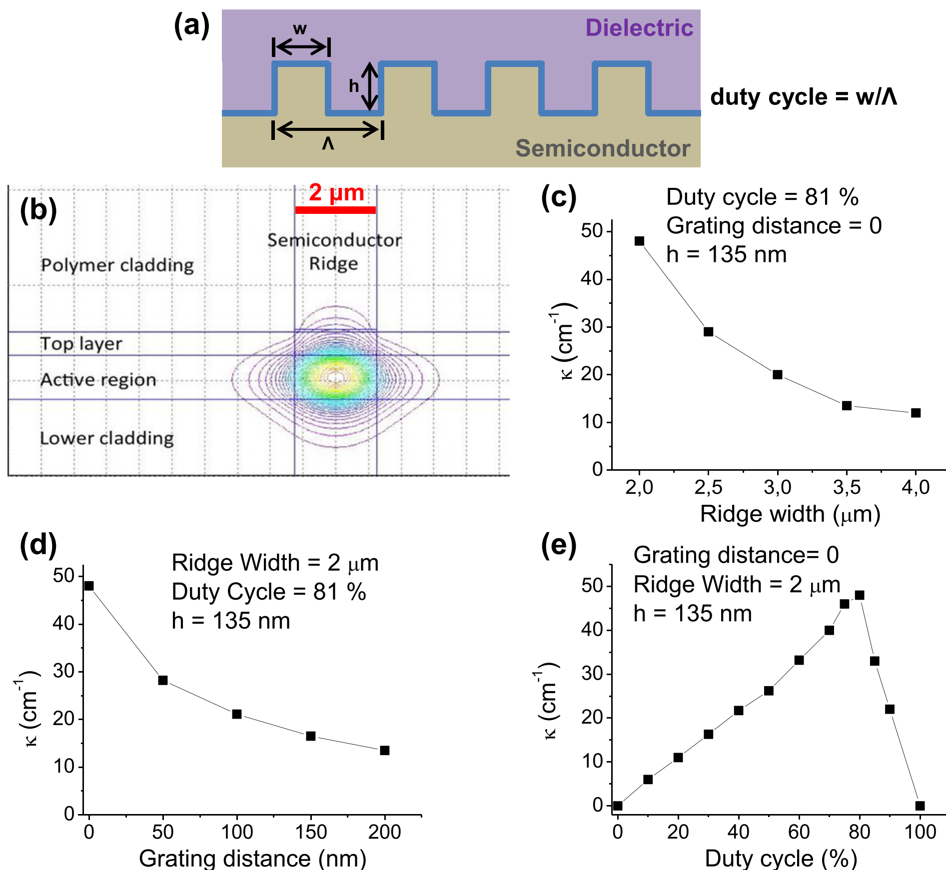

FIG. 1. Calculation of the coupling coefficient κ, as a function of the most critical laser design parameters affecting its value: (a) schematic representation of the parameter w that was varied in the numerical analysis determining the κ dependence on the Bragg grating duty cycle value. The Bragg grating period Λ has been fixed in order to determine the emission wavelength of the laser to match the NH_3 absorption line, centered at 1.982 μm. (b) Calculated fundamental quasi-TE mode profile of a Qdash laser emitting at 2 μm. (c) κ dependence on the ridge waveguide width. (d) κ dependence on the grating proximity to the ridge. (e) κ dependence on the Bragg grating duty cycle.

RIGHTSLINK

2 μm laser is shown in Fig. 1(b). To further improve the computational efficiency, during this step, the grating layer has been approximated by a homogeneous layer of a weighted refractive index.[13] A detailed theoretical analysis for LC-DFB lasers using a similar approach to the one followed here is provided by Choi *et al*.[45] As shown in Fig. 1(c), an important parameter affecting κ is the ridge width, a result expected intuitively, since a narrow ridge would result in a bigger portion of the optical mode spread out of the ridge, into the Bragg grating region. However, reducing the ridge width too much is not advisable as it will result in a high electrical resistance,[46] a reduced output power, increased intra-cavity losses, and non-well-controlled κ values affecting the reproducibility of the process for small fabrication differences.[42] Taking these trade-offs into account, a 2 μm wide ridge is adopted in our devices. Figure 1(d) shows the κ dependence on the grating proximity to the ridge. This result underlines the importance of achieving a high verticality of the waveguide, as well as the high accuracy alignment for integrating the different steps of the LC-DFB fabrication process, as a small grating misplacement of a few nm may cause a substantial κ reduction. This could be of the order of 20% reduction for only 5 nm misalignments, or a factor of 2 for 50 nm misalignments. Finally, Figure 1(e) underlines the fact that optimizing the grating duty cycle is an important parameter that was not taken into account in previous experimental LC-DFB works, which utilized duty cycles of 50% or less. This may lead to an important coupling improvement by simply adjusting a single step in the process flow. The intuitive understanding of the importance of increasing the duty cycle value arises by the fact that, while this reduces the sine term of Eq. (1), it increases the weighted refractive index of the grating, attracting a higher portion of the optical mode into the grating region, thus increasing $\Gamma_{grating}$. Therefore, these two terms need to be maximized simultaneously in Eq. (1), and the optimum values depend on the pair of the refractive indices of the materials used to compose the Bragg grating. For our structure, the optimum duty cycle value is ~80%.

IV. LC-DFB LASER FABRICATION

For the implementation of this design, we have developed a novel process specifically designed to achieve a high and well-control coupling coefficient. First, 1.9 μm wide stripes of Ti/Au/Cr (200/2000/100 Å) were defined using electron beam lithography (EBL) and a liftoff process. The alignment marks have also been defined during this step. Subsequently, using a second EBL step, aligned with the first one, 2.0 μm wide hydrogen silsesquioxane (HSQ) trenches of ~300 nm thickness were placed on top of the metallic ones, in order to serve as a mask for the waveguide definition. An SEM top view image after HSQ development is depicted in Fig. 2(a). The reason for this alignment step is that it is desirable to ultimately have a metallic layer on top of the ridge, in order to facilitate current injection. It would also be possible to deposit a Ti/Au layer on top of the whole wafer and subsequently etch it together with the semiconductor layers to define a ridge with Au on top, but successive dry etching of Au/InGaAs/InP layers is difficult to result in a smooth surface and sidewall. By protecting the metallic layer under the HSQ mask, we can ensure a good etching quality of the semiconductor. Fig. 2(b) depicts a cross-sectional SEM view after etching of the InGaAs ohmic contact and InP cladding layers using a Cl_2-based inductively coupled plasma (ICP) process. During this step, it is very important to stop the etching ~50–70 nm above the quaternary layer dedicated for the Bragg grating fabrication. For this reason, the process is monitored using *in-situ* interferometry (Fig. 2(c)) and is subsequently tested using cross-sectional images taken from small parts of the sample (Fig. 2(d)). Then, the remaining InP cladding in the ridge vicinity (Fig. 2(d)) is removed using a selective HCl/H_3PO_4 (ratio 1:4) wet-etching step. Using a third EBL alignment step, high-duty-cycle Bragg gratings of 375 μm length, and a grating period of $\Lambda = 276$ nm with 60-nm-wide openings, have been defined on a SiN_x mask on both sides of the ridge waveguide. The grating length has been designed to be shorter than the cavity length, in a similar manner to the work of Li and Cheng[29] in order to achieve optimized normalized coupling coefficient κL values. We targeted a value of $\kappa L \sim 1.5$, slightly higher than the designed values in conventional DFB lasers ($\kappa L \sim 1$–1.25). The reason for this has been to ensure high SMSR without employing neither a phase-shift nor anti-reflection (AR) coatings to the laser, in order to maintain a simplified low-cost process, benefitting by the fact that the spatial hole burning effect is not severe in our LC-DFBs for such κL values, as also confirmed by our results. The pattern was then transferred into the 35 nm thick $In_{0.78}Ga_{0.22}As_{0.47}P_{0.53}$ quaternary layer, using a $CH_4/H_2/O_2$ reactive ion etching (RIE) process at a low etch rate (~120 nm/min). SEM cross-sectional images of the steps followed for the high-duty-cycle Bragg grating optimization are presented in Fig. 3. Fig. 3(a) shows a test Bragg grating after RIE. Before removing the sample from the reactor, oxygen cleaning takes place in order to achieve a smooth grating sidewall (Fig. 3(b)), to reduce scattering losses. Fig. 3(c) depicts a Bragg grating with narrow gaps of ~60 nm achieved after optimization of the EBL parameters. After the grating definition, the remaining masks are removed using an RIE SF_6 process and then benzocyclobutene (BCB) resign is spin coated in order to provide the mechanical support and electrical isolation for the ridges. This dielectric also penetrates into the Bragg grating gaps and serves as the n_2 material in Eq. (1). Figs. 3(d)–3(f) show zoom-in and zoom-out cross-sectional SEM images, confirming that the BCB correctly and uniformly enters the gratings' gaps. Subsequently, the BCB film on top of the current injection region was opened using an RIE O_2/SF_6 gas mixture and 100 μm wide Ti/Au electrical contacts were deposited onto the p-side of the wafer using an optical lithography and the lift-off process. After thinning the wafer down to ~100 μm, electrical contacts were deposited on the back-side of the wafer as well. Then, the remaining BCB between the contacts was removed using RIE to facilitate the device cleavage, and lasers were cleaved and mounted n-side down onto Cu heat sinks with as-cleaved facets.

V. RESULTS AND DISCUSSION

For the optical study of the lasers, a conventional free space measurement setup was utilized. The lasers were

RIGHTSLINK Copyright Clearance Center

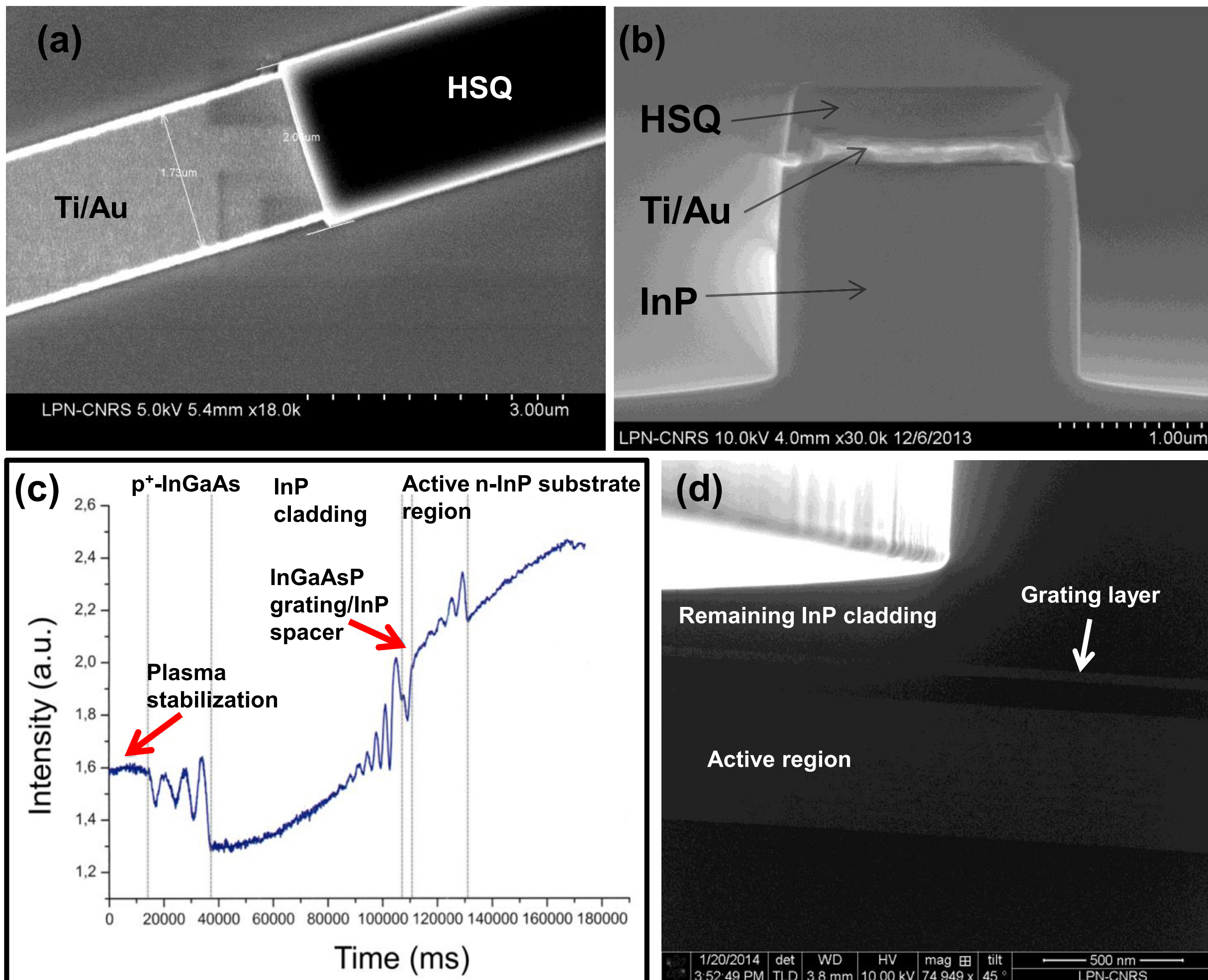

FIG. 2. (a) SEM top view of the first alignment process for the definition of the 1.9 μm-wide Ti/Au layers and the 2.0 μm-wide HSQ mask, used for the definition of the ridge waveguide. (b) Pattern transferred to the InP cladding layer using a Cl_2-based ICP process at high etch rate. (c) The process was controlled using *in situ* interferometry, in order to accurately interrupt the etching 50–70 nm above the thin epitaxial layer designed for the definition of the Bragg grating. (d) SEM cross-sectional view of a ridge waveguide after the ICP process. The remaining thin cladding layer shown was subsequently removed using a selective wet etching step.

thermally stabilized at 20 °C on a Peltier element stage and were operated under CW electrical pumping. CaF_2 lenses provided coupling to a 1 m monochromator, equipped with the extended InGaAs detector operating in the 0.9–2.6 μm spectral range. The spectral resolution of the setup is <80 pm at 2 μm, which is sufficient for laser transverse mode detection. The laser spectra for two samples A and B, with cavity lengths of 630 and 910 μm, are presented in Figs. 4 and 5, respectively. The spectra indicate the single mode operation with the side mode suppression >37 dB for sample A and >29 dB for sample B. These are suitable for narrow gas line detection. Threshold currents of 65 and 110 mA have been measured, as shown in the LI curves in the top right corner insets of the graphs. The lasers exhibit a maximum output power per facet of 4.5 mW and 5.5 mW, respectively. The slope efficiency in these LI curves is approximately 0.25 W/A and 0.15 W/A. This corresponds to an estimation for the external differential quantum efficiency (n_{ext}) of 0.4 and 0.24, respectively, for these lasers. Threshold current (I_{th}) and output power (P_{out}) value comparison between our LC-DFBs and ridge-waveguide lasers obtained from the same epi-wafer confirms the negligible grating-induced additional losses in our design. Laser tunability is provided by the temperature control and is depicted for both samples in the top left insets of the graphs. Sample B was manufactured for NH_3 gas detection. Fig. 6 provides sample B laser emission at 15 °C and 20 °C overlaid on top of the NH_3 absorption spectrum. The absorption spectrum of NH_3 was taken from the HITRAN database.[47] According to the laser peak temperature dependence, at T = 13 °C, the laser peak overlaps with an intensive absorption line of NH_3. Under these conditions, sample B can be efficiently utilised for gas detection—stable reference intensity can be acquired at 23 °C and gas sensitive measurements can be performed at 13 °C. These results indicate that our design combines stable single-mode operation with a high SMSR already for short gratings, while maintaining low losses. The latter has been achieved by avoiding the main loss sources of the conventional approaches: namely, the highly absorbing metal gratings in LC-DFB designs[48] and the gratings formed on the ridge or on the ridge sidewalls in CRW designs that result in lower lateral optical confinement and increased carrier diffusion into the gratings teeth. A relative ease of fabrication is evident as compared to the conventional DFB processes with

RIGHTSLINK

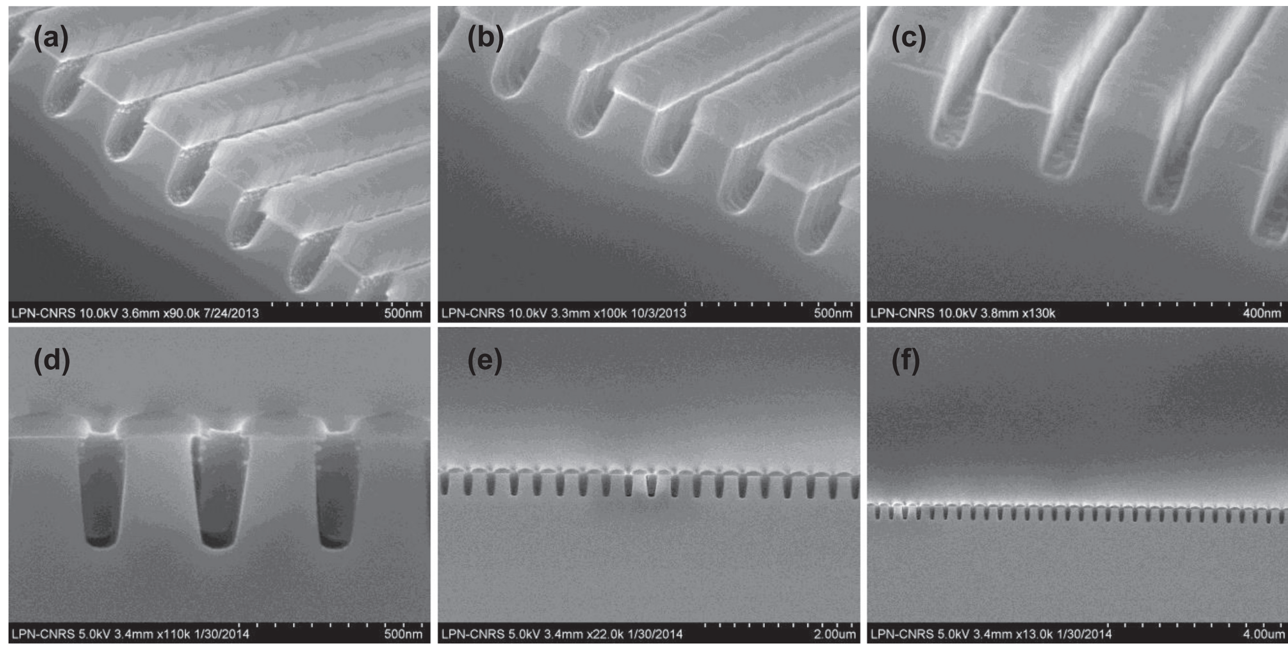

FIG. 3. SEM images taken during the optimization of the processing steps for the high-duty-cycle Bragg grating: (a) Bragg grating etched using an RIE CH_4-H_2 process at low etch rate, which enables very accurate control of the grating depth. (b) The grating sidewalls quality improved after oxygen cleaning of the sample insight the RIE reactor after the etching was completed. (c) Vertical sidewalls and the targeted duty cycle value were achieved after optimizing the e-beam lithography parameters and the CH_4/H_2 ratio during RIE. (d) SEM confirmation that the spin-coated BCB dielectric penetrates into the 60-nm-wide narrow trenches of the Bragg grating. (e) and (f) Zoom-out cross-sectional SEM views at different positions confirm the correct grating definition over the whole region covered by the optimized high-duty-cycle Bragg gratings.

buried gratings, which require complex, high-cost steps, such as epitaxial grating overgrowth and Bragg-grating formation on a non-planar surface. Good wavelength controllability is preserved in both our novel growth approach resulting in the required gain peak and our fabrication process, resulting in the desired single mode selection for the targeted gas detection.

The temperature coefficient is estimated at 0.04 nm/K and 0.07 nm/K for samples A and B, respectively. The temperature coefficient of sample B could be evaluated in agreement with experimental values previously reported in the literature for InP based DFB and DBR lasers, in similar material systems. For comparison, we note that a temperature coefficient of 0.092 nm/K has been measured in 1.55 μm GaInAsP/InP LC-DBR lasers,[49] while values of 0.11 nm/K and 0.14 nm/K have been extracted for AlGaInAs/InAs/InP Qdash based LC-DFB lasers emitting at 1.55 μm (Ref. 50) and 2 μm (Ref. 9), respectively, and 0.11 nm/K for InGaAs/InGaAsP QW based DFB lasers at 1.95 μm.[51] Sb-based LC-DFB lasers emitting at 2 μm have been found to exhibit a somewhat larger temperature coefficient of 0.2 nm/K.[13] We believe that the observed difference in the temperature coefficient of our sample A is mainly due to the fact that the Bragg grating of this laser is negatively detuned. Also, slight discrepancies may be attributed to the fact that our lasers operated in a limited temperature range,

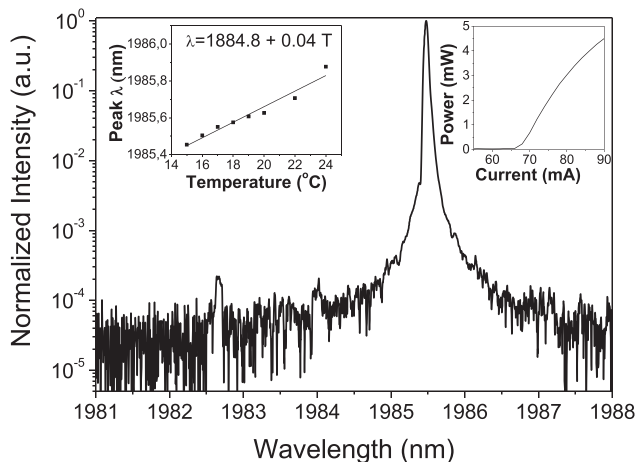

FIG. 4. Room temperature single mode spectrum of sample A (L = 630 μm) with CW drive current of I = 100 mA. The lasing wavelength is 1985.6 nm with 37 dB SMSR. Insets show a peak shift with temperature and L-I curve.

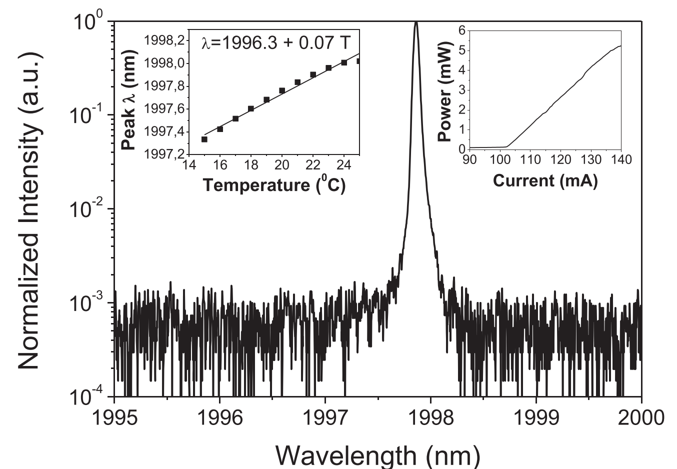

FIG. 5. Room temperature single mode spectrum of sample B (L = 910 μm) with CW drive current of I = 120 mA. The lasing wavelength is 1997.8 nm with 29 dB SMSR. Insets show a peak shift with temperature and L-I curve.

RIGHTSLINK

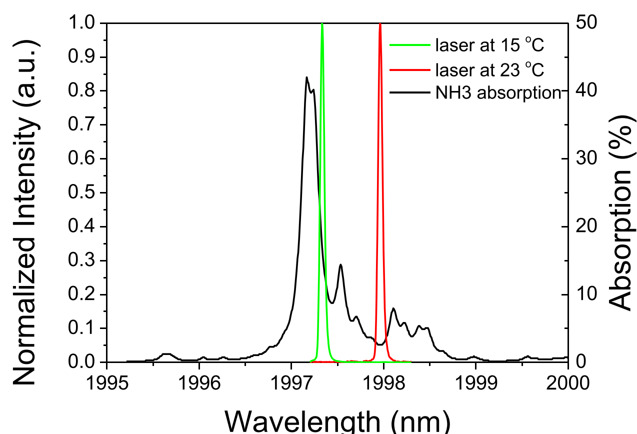

FIG. 6. NH_3 (10 cm, 1 bar, 20 °C) gas cell theoretical absorption spectrum versus spectrum of sample B LC-DFB laser operating at 15 °C and 23 °C.

and we therefore have a somewhat limited fitting accuracy. In any case, our estimated temperature coefficient values confirm that our lasers operated via the DFB mode, as the wavelength shift is governed by the temperature dependence of the effective refractive index of the waveguide, rather than the gain peak (energy gap) shift. Fabry-Perot (FP) lasing modes are expected to appear in our device under certain biasing and temperature conditions. Under the conditions reported above (I = 100 mA in Fig. 4, I = 120 mA in Fig. 5; at room temperature), the spectra show no FP lasing modes. With increased current injection (or at high temperature operation), the higher tuning rate of the gain spectrum in comparison to the DFB mode leads to laser oscillation in FP modes away from the Bragg wavelength. It is worth mentioning that in DFB lasers with as-cleaved facets having a κL value between one and two, of the order of our devices, single longitudinal mode lasing may be maintained in a relatively wide window of current injection and temperature operation, as determined by the relation of the net gain spectra with the relative loss difference between DFB and FP modes in such devices. The transition from DFB to Fabry Perot operation in such as-cleaved DFB lasers is definitely of interest; however, it is beyond the scope of the current article. On the other hand, the FP fringes are not observed in our spectra with >37 dB and >29 dB SMSR, due to the lower detector sensitivity in the 2 μm wavelength range. It is also worth mentioning that for a real sensing environment, a higher temperature operation would be highly beneficial. Our lasers (both the DFB and FP lasers that were tested) only operated over a limited temperature range as shown above. This suggests that further bandgap engineering optimisation can be employed in our experimental growth approach, where we have tested the lowest available barrier that is lattice matched to InP (ternary $In_{0.53}Ga_{0.47}As$). It turns out that this barrier material would be optimum for longer wavelength emission, which is a milestone for quantum dash InP(001) based lasers and would be highly desirable. At the current study, focussing at an emission wavelength around 2 μm, the lasers operate fairly well and exhibit a relatively low I_{th}; however, such a low barrier is not the optimum for high-temperature operation. This is because the conduction band offset between the Qdash and the $In_{0.53}Ga_{0.47}As$ barrier turns out to be not sufficiently high, leading to fast thermal roll-over at higher temperatures and also for high current injection. In future work, lasers emitting at 2 μm will be investigated using an intermediate quaternary barrier, while the ternary barrier of the current approach will be utilized to achieve high-performance lasing at longer wavelengths.

VI. CONCLUSIONS

In conclusion, we investigated an alternative approach to achieve high and well-controlled κ values for single mode DFB operation that combines the wavelength performance of conventional DFB lasers with the simplified fabrication process of LC-DFB lasers. The concept of high-duty-cycle Bragg gratings is introduced experimentally for the first time and tested in a fabricated functioning device. We show that such Bragg gratings appreciably increase the coupling coefficient of an LC-DFB laser, by achieving an SMSR > 37 dB, $\kappa \sim 40\,cm^{-1}$ while enabling substantially low grating-induced losses, which was confirmed by comparing key laser performances, such as the I_{th} and P_{out} between our LC-DFBs and ridge-waveguide lasers fabricated from the same epi-wafer. As a result, sufficient mode selection using a moderately short grating segment is achieved, which is an important step towards the realization of high-performance LC-DBR lasers. In terms of the material quality, our results open the way for the fabrication of Qdash based lasers emitting above 2 μm, as a result of the successful implementation of the InGaAs ternary barriers, aiming to cover a larger wavelength range using the technologically favorable InP(001) material system and low-dimensional nanostructures.

ACKNOWLEDGMENTS

This work was supported by EU FP7 ITN PROPHET, Grant No. 264687 and in part by Science Foundation Ireland (SFI), under the USIreland R&D Partnership Programme Grant No. SFI/14/US/I3057. The authors acknowledge Dr. Andrea Cattoni for fruitful discussions about the e-beam lithography process.

[1]A. Somers, W. Kaiser, J. P. Reithmaier, A. Forchel, M. Gioaninni, and I. Montrosset, Appl. Phys. Lett. **89**, 061107 (2006).
[2]W. Zeller, M. Legge, J. Seufert, R. Werner, M. Fischer, and J. Koeth, Appl. Opt. **48**, B51 (2009).
[3]J. P. Reithmaier, A. Somers, S. Deubert, R. Schwertberger *et al.*, J. Phys. D: Appl. Phys. **38**, 2088–2102 (2005).
[4]K. Papatryfonos, G. Rodary, C. David, F. Lelarge, A. Ramdane, and J. C. Girard, Nano Lett. **15**(7), 4488–4497 (2015).
[5]F. Lelarge, B. Dagens, J. Renaudier, R. Brenot, A. Accard, F. van Dijk, D. Make, O. Le Gouezigou, J.-G. Provost, F. Poingt, J. Landreau, O. Drisse, E. Derouin, B. Rousseau, F. Pommereau, and G.-H. Duan, IEEE J. Sel. Top. Quantum Electron. **13**(1), 111–124 (2007).
[6]R. Rosales, S. G. Murdoch, R. T. Watts, K. Merghem, A. Martinez, F. Lelarge, A. Accard, L. P. Barry, and A. Ramdane, Opt. Express **20**(8), 8649–8657 (2012).
[7]O. Mollet, A. Martinez, K. Merghem, S. Joshi, J.-G. Provost, F. Lelarge, and A. Ramdane, Appl. Phys. Lett. **105**, 141113 (2014).
[8]S. Hein, A. Somers, W. Kaiser, S. Höfling, J. P. Reithmaier, and A. Forchel, Electron. Lett. **44**(8), 527–528 (2008).
[9]W. Zeller, M. Legge, A. Somers, W. Kaiser, J. Koeth, and A. Forchel, Electron. Lett. **44**, 354–355 (2008).

RIGHTSLINK

[10]K. Papatryfonos, S. Joshi, K. Merghem, S. Bouchoule, S. Guilet, L. Le Gratiet, A. Martinez, and A. Ramdane, in IEEE 26th International Conference on Indium Phosphide and Related Materials (IPRM) (2014).
[11]Ł. Dusanowski, M. Syperek, J. Misiewicz, A. Somers, S. Höfling, M. Kamp, J. P. Reithmaier, and G. Sęk, Appl. Phys. Lett. **108**, 163108 (2016).
[12]A. Sauerwald, T. Kummell, G. Bacher, A. Somers, R. Schwertberger, J. P. Reithmaier, and A. Forchel, Appl. Phys. Lett. **86**, 253112 (2005).
[13]S. Forouhar, R. M. Briggs, C. Frez, K. J. Franz, and A. Ksendzov, Appl. Phys. Lett. **100**, 031107 (2012).
[14]S. Belahsene, L. Naehle, M. Fischer, J. Koeth, G. Boissier, P. Grech, G. Narcy, A. Vicet, and Y. Rouillard, IEEE Photonics Technol. Lett. **22**, 1084 (2010).
[15]S. Sprengel, C. Grasse, K. Vizbaras, T. Gruendl, and M. C. Amann, Appl. Phys. Lett. **99**, 221109 (2011).
[16]S. Sprengel, A. Andrejew, K. Vizbaras, T. Gruendl, K. Geiger, G. Boehm, C. Grasse, and M. C. Amann, Appl. Phys. Lett. **100**, 041109 (2012).
[17]T. Sato, M. Mitsuhara, N. Nunoya, T. Fujisawa, K. Kasaya, F. Kano, and Y. Kondo, IEEE Photonics Technol. Lett. **20**(12), 1045–1047 (2008).
[18]Z. L. Liau, D. C. Flanders, J. N. Walpole, and N. DeMeo, Appl. Phys. Lett. **46**(3), 221–223 (1985).
[19]L. M. Miller, J. T. Verdeyen, J. J. Coleman, R. P. Bryan, J. J. Alwan, K. J. Beernink, J. S. Hughes, and T. M. Cockerill, IEEE Photonics Technol. Lett. **3**(1), 6–8 (1991).
[20]R. D. Martin, S. Forouhar, S. Keo, R. J. Lang, R. G. Hunsperger, R. C. Tiberio, and P. F. Chapman, IEEE Photonics Technol. Lett. **7**(3), 244–246 (1995).
[21]N. Chen, Y. Watanabe, K. Takei, and K. Chikuma, Jpn. J. Appl. Phys., Part 1 **39**(3B), 1508–1511 (2000).
[22]M. Kamp, J. Hofmann, A. Forchel, F. Schafer, and J.-P. Reithmaier, Appl. Phys. Lett. **74**, 483–485 (1999).
[23]M. Muller, M. Kamp, A. Forchel, and J.-L. Gentner, Appl. Phys. Lett. **79**, 2684–2686 (2001).
[24]T. Lehnhardt, M. Hümmer, K. Rößner, M. Müller, S. Höfling, and A. Forchel, Appl. Phys. Lett. **92**, 183508 (2008).
[25]J. A. Gupta, P. J. Barrios, J. Lapointe, G. C. Aers, and C. Storey, Appl. Phys. Lett. **95**, 041104 (2009).
[26]S. Forouhar, C. Borgentun, C. Frez, R. M. Briggs, M. Bagheri, C. L. Canedy, C. S. Kim, M. Kim, W. W. Bewley, C. D. Merritt, J. Abell, I. Vurgaftman, and J. R. Meyer, Appl. Phys. Lett. **105**, 051110 (2014).
[27]Y. Watanabe, N. Chen, K. Takei, K. Chijuma, N. Futakuchi, and Y. Nakano, IEEE Photonics Technol. Lett. **10**(12), 1688–1690 (1998).
[28]T. J. Slight, G. Tandoi, D. G. Revin, A. McKee, S. Y. Zhang, W. Meredith, J. W. Cockburn, and C. N. Ironside, IEEE Photonics Technol. Lett. **23**(7), 420–422 (2011).
[29]J. Li and J. Cheng, Electron. Lett. **49**(12), 764–766 (2013).
[30]R. Millett, K. Dridi, A. Benhsaien, H. Schriemer, K. Hinzer, and T. Hall, Photonics Nanostruct.: Fundam. Appl. **9**(2), 111–118 (2011).
[31]A. Akrout, K. Dridi, and T. J. Hall, IEEE J. Quantum Electron. **48**, 1252–1258 (2012).
[32]K. Dridi, A. Benhsaien, J. Zhang, and T. J. Hall, IEEE Photonics Technol. Lett. **26**(12), 1192–1195 (2014).
[33]K. Dridi, A. Benhsaien, J. Zhang, K. Hinzer, and T. J. Hall, Opt. Express **22**(16), 19087–19097 (2014).
[34]K. Dridi, A. Benhsaien, J. Zhang, and T. J. Hall, Opt. Lett. **39**(21), 6197–6200 (2014).
[35]H. Konig, S. Rennon, J. P. Reithmaier, A. Forchel, J. L. Gentner, and L. Goldstein, Appl. Phys. Lett. **75**(11), 1491–1493 (1999).
[36]L. Bach, S. Rennon, J. P. Reithmaier, A. Forchel, J. L. Gentner, and L. Goldstein, IEEE Photonics Technol. Lett. **14**(7), 1037–1039 (2002).
[37]L. Bach, W. Kaiser, J. P. Reithmaier, A. Forchel, M. Gioannini, V. Feies, and I. Montrosset, IEEE Photonics Technol. Lett. **16**(1), 18–20 (2004).
[38]M. J. Strain and M. Sorel, IEEE Photonics Technol. Lett. **18**(24), 2566–2568 (2006).
[39]M. J. Strain and M. Sorel, IEEE Photonics Technol. Lett. **20**(22), 1863–1865 (2008).
[40]J. Dong, A. Ubukata, and K. Matsumoto, IEEE Photonics Technol. Lett. **10**(4), 513–515 (1998).
[41]W. Lei, H. H. Tan, and C. Jagadish, Appl. Phys. Lett. **96**, 213102 (2010).
[42]K. Papatryfonos, Ph.D. thesis, Optics/Photonic. Institut national des Télécommunications, Paris, France, 2015, pp. 81–84, 103–105.
[43]J. X. Kong, Q. S. Zhu, B. Xu, and Z. G. Wang, J. Appl. Phys. **109**, 084345 (2011).
[44]G. P. Agrawal and N. K. Dutta, *Long-Wavelength Semiconductor Lasers* (Van Nostrand, New York, 1968), pp. 305–305.
[45]W. Y. Choi, J. C. Chen, and C. G. Fonstad, Jpn. J. Appl. Phys., Part 1 **35**, 4654–4659 (1996).
[46]J. Wang, J. B. Tian, P. F. Cai, B. Xiong, C. Z. Sun, and Y. Luo, IEEE Photonics Technol. Lett. **17**(7), 1372–1374 (2005).
[47]L. S. Rothman, I. E. Gordon, Y. Babikov, A. Barbe, D. C. Benner, P. F. Bernath *et al.*, J. Quant. Spectrosc. Radiat. Transfer **130**, 4–50 (2013).
[48]A. Salhi, D. Barat, D. Romanini, Y. Rouillard, A. Ouvrard, R. Werner, J. Seufert, J. Koeth, A. Vicet, and A. Garnache, Appl. Opt. **45**(20), 4957–4965 (2006).
[49]S. Rennon, L. Bach, J. P. Reithmaier, and A. Forchel, IEEE J. Sel. Top. Quantum Electron. **7**, 306–311 (2001).
[50]W. Kaiser, K. Mathwig, S. Deubert, J. P. Reithmaier, A. Forchel, O. Parillaud, M. Krakowski, D. Hadass, V. Mikhelashvili, and G. Eisenstein, Electron. Lett. **41**(14), 808–810 (2005).
[51]J. Dong, A. Ubukata, and K. Matsumoto, Electron. Lett. **33**(12), 1090–1092 (1997).

RIGHTSLINK